AGU PUBLICATIONS

Geophysical Research Letters

RESEARCH LETTER
10.1002/2015GL063960

Key Points:
- We predict sea level changes associated with a model of North American deglaciation
- A North American ice saddle collapse may have been the dominant source of MWP-1A
- We draw our conclusions on the basis of fits to far-field sea level records

Correspondence to:
N. Gomez,
ngomez@cims.nyu.edu

Citation:
Gomez, N., L. J. Gregoire, J. X. Mitrovica, and A. J. Payne (2015), Laurentide-Cordilleran Ice Sheet saddle collapse as a contribution to meltwater pulse 1A, *Geophys. Res. Lett.*, *42*, 3954–3962, doi:10.1002/2015GL063960.

Received 23 MAR 2015
Accepted 16 APR 2015
Accepted article online 21 APR 2015
Published online 22 MAY 2015

Laurentide-Cordilleran Ice Sheet saddle collapse as a contribution to meltwater pulse 1A

N. Gomez[1], L. J. Gregoire[2], J. X. Mitrovica[3], and A. J. Payne[4]

[1]Center for Atmosphere Ocean Sciences, Courant Institute for Mathematical Sciences, New York University, New York, New York, USA, [2]School of Earth and Environment, University of Leeds, Leeds, UK, [3]Earth and Planetary Sciences, Harvard University, Cambridge, Massachusetts, USA, [4]Centre for Polar Observation and Modelling, School of Geographical Sciences, University of Bristol, Bristol, UK

Abstract The source or sources of meltwater pulse 1A (MWP-1A) at ~14.5 ka, recorded at widely distributed sites as a sea level rise of ~10–20 m in less than 500 years, is uncertain. A recent ice modeling study of North America and Greenland has suggested that the collapse of an ice saddle between the Laurentide and Cordilleran ice sheets, with a eustatic sea level equivalent (ESLE) of ~10 m, may have been the dominant contributor to MWP-1A. To test this suggestion, we predict gravitationally self-consistent sea level changes from the Last Glacial Maximum to the present day associated with the ice model. We find that a combination of the saddle collapse scenario and melting outside North America and Greenland with an ESLE of ~3 m yields sea level changes across MWP-1A that are consistent with far-field sea level records at Barbados, Tahiti, and Sunda Shelf.

1. Introduction

The deglaciation phase of the last glacial period was punctuated by meltwater pulses associated with the rapid collapse of ice sheet sectors [e.g., *Fairbanks*, 1989; *Bard et al.*, 2010; *Deschamps et al.*, 2012]. Perhaps the most prominent example is meltwater pulse 1A (MWP-1A) at ~14.5 ka, which involved ~15 m of eustatic sea level rise in less than 340 years [*Deschamps et al.*, 2012].

The source or sources of MWP-1A are uncertain. It has been assumed that retreat of the Laurentide ice sheet (LIS) [*Kennett and Shackleton*, 1975; *Fairbanks et al.*, 1992], and in particular the southern sector of the ice sheet [*Leventer et al.*, 1982; *Keigwin and Jones*, 2010; *Andrews et al.*, 1994; *Peltier*, 2004], dominated the meltwater flux. However, a significant southern Laurentian source for MWP-1A is inconsistent with recent analyses of oxygen isotope records from the Gulf of Mexico [*Carlson*, 2009; *Wickert et al.*, 2013]. Moreover, analysis of sea level records across the MWP-1A time window at Barbados [*Fairbanks*, 1989; *Bard et al.*, 1990] and Sunda Shelf [*Hanebuth et al.*, 2000] appears to rule out a sole southern LIS source [*Clark et al.*, 2002].

The sea level fingerprinting study of *Clark et al.* [2002] suggests a variety of alternate scenarios for MWP-1A, including globally distributed sources or a dominant contribution from the Antarctic ice sheet (AIS). The latter suggestion is supported by climate modeling [*Weaver et al.*, 2003], an analysis of far-field sea level records during the post-MWP-1A time period [*Bassett*, 2005], and a fingerprinting study including newly collected sea level data from Tahiti [*Deschamps et al.*, 2012]. In contrast, a relatively minor contribution from the AIS to MWP-1A is indicated by recent AIS modeling studies [*Whitehouse et al.*, 2012; *Ivins et al.*, 2013; *Gomez et al.*, 2013; *Briggs et al.*, 2014; *Golledge et al.*, 2014].

Recently, *Gregoire et al.* [2012] (henceforth G12) modeled the retreat of the LIS, the Cordilleran Ice Sheet (CIS), and the Greenland Ice Sheet (GIS) from Last Glacial Maximum (LGM) to the present day. They concluded that the collapse of the ice saddle between the LIS and CIS might have been responsible for a significant component of MWP-1A. The consistency of their scenario with observations of the sea level change across the MWP-1A time window has not been explored. In this study, we compute the post-LGM sea level change using the G12 model and compare the predictions with available sea level records across the MWP-1A window. We begin by summarizing these records.

2. Methods

2.1. Far-Field Constraints on the Sea Level Rise Across MWP-1A

Observational constraints on the change in sea level across the MWP-1A event exist at three sites: Barbados, Tahiti, and Sunda Shelf. *Deschamps et al.* [2012] estimated the sea level rise at Tahiti to be 12–22 m in less than

340 years, with a preferred range of 14–18 m. They also reevaluated the coral record of sea level change across the MWP-1A time window at Barbados by extrapolating trends from two cores that bound the timing of MWP-1A, finding that an event of duration of 100–340 years suggests a local sea level rise of 14–18 m (see their Figure S7 and associated discussion). *Hanebuth et al.* [2000] estimated a sharp sea level rise of up to 16 m within 300 years across the MWP-1A time window at Sunda Shelf on the basis of core records of mangrove organic material. However, this estimate was bounded by data from cores collected at different geographic sites, and correcting the record for spatial gradients in the sea level response yields a revised estimate of 7–17 m [*Liu et al.*, 2013; Glenn Milne, personal communication, January 6, 2015].

2.2. Sea Level Modeling

We compute postglacial sea level changes using a gravitationally self-consistent theory that accounts for viscoelastic deformation of the solid Earth, migrating shorelines, and the feedback into sea level of perturbations in Earth rotation [*Kendall et al.*, 2005]. We adopt a 1-D (depth varying) Maxwell Earth model with a truncation at spherical harmonic degree 256. The elastic and density structure of the Earth model is prescribed by the seismic model preliminary reference Earth model [*Dziewonski and Anderson*, 1981]. We consider two different radial profiles of mantle viscosity. The first, the VM2 model of *Peltier* [2004], which is associated with the ICE-5G global ice history reconstruction, has a 90 km thick elastic lithosphere, upper mantle viscosity close to 5×10^{20} Pa s, and a lower mantle viscosity that remains close to $2–3 \times 10^{21}$ Pa s. The second, henceforth model LM, has a lithospheric thickness of 70 km and upper and lower mantle viscosities of 2×10^{20} Pa s and 10^{22} Pa s, respectively. The latter model is among a class of models preferred on the basis of independent analyses of ice age data sets [e.g., *Lambeck et al.*, 2014; *Mitrovica and Forte*, 2004].

We quantify the contribution from different ice sources to MWP-1A in terms of a "eustatic sea level equivalent" (ESLE). Following *Gomez et al.* [2010], the ESLE is the globally uniform shift in sea level that yields a volume equal to the meltwater volume, after the latter has been corrected to fill marine-based sectors exposed by the melting ice sheets. In some results below, we normalize predicted sea level changes by the ESLE to produce "sea level fingerprints" that highlight the geometry of the sea level patterns associated with different meltwater sources and scale and sum the contributions from different fingerprint patterns in order to compare modeling results with sea level observations.

2.3. Ice Histories

The G12 model for the LIS, CIS, and GIS extends from LGM (21 ka) to present, and we compute postglacial sea level changes across this entire period. Figure 1a shows the meltwater flux associated with changes in grounded ice over a time window that encompasses the collapse of the ice saddle between the LIS and CIS. The flux peaks at ~0.30 sverdrup (Sv) during this interval, with a background flux of ~0.1–0.15 Sv. Figures 1b and 1c show snapshots of the ice cover at model times 11.8 ka and 11.3 ka, which bound the main phase of saddle collapse. The ice collapse across this interval is focused in northwestern Canada, but ice cover also thins in the vicinity of Hudson Bay.

G12 interpret the model time window of 11.8–11.3 ka, which corresponds to an ESLE of 10.47 m, as coinciding with the main phase of MWP-1A (i.e., 14.5–14 ka) on the basis that the timing of MWP-1A is consistent with the analyses of geochronological constraints on the opening of an ice-free corridor between the LIS and CIS [*Dyke*, 2004; *Munyikwa et al.*, 2011]. However, there remains significant uncertainty in these constraints, and a scenario in which the opening of this corridor preceded MWP-1A is also consistent with these analyses. Further constraints are needed to unambiguously distinguish between these two scenarios.

The observed change in sea level during the MWP-1A event will contain a background contribution from ice geometry variations outside of the G12 model domain. We prescribe these sea level changes by adopting the ICE-5G ice model in regions outside of North America and Greenland from LGM to the present. This component of the ICE-5G reconstruction includes melting across the MWP-1A window (14.5–14 ka) with an ESLE of ~1.3 m sourced to Eurasian and Patagonian ice cover.

The ICE-5G reconstruction has negligible ice loss in Antarctica leading up to and during MWP-1A. To consider the impact on sea level of a contribution to MWP-1A from Antarctica, we adopt the ice loss geometry in the coupled AIS—sea level model of *Gomez et al.* [2013] from 14.5 to 14 ka (ESLE ~1 m). We neglect the viscous component of the contribution from the AIS melting because *Gomez et al.*'s [2013] model has negligible pre-MWP-1A melting, and the sea level change at sites in the far field of the last glacial period ice cover

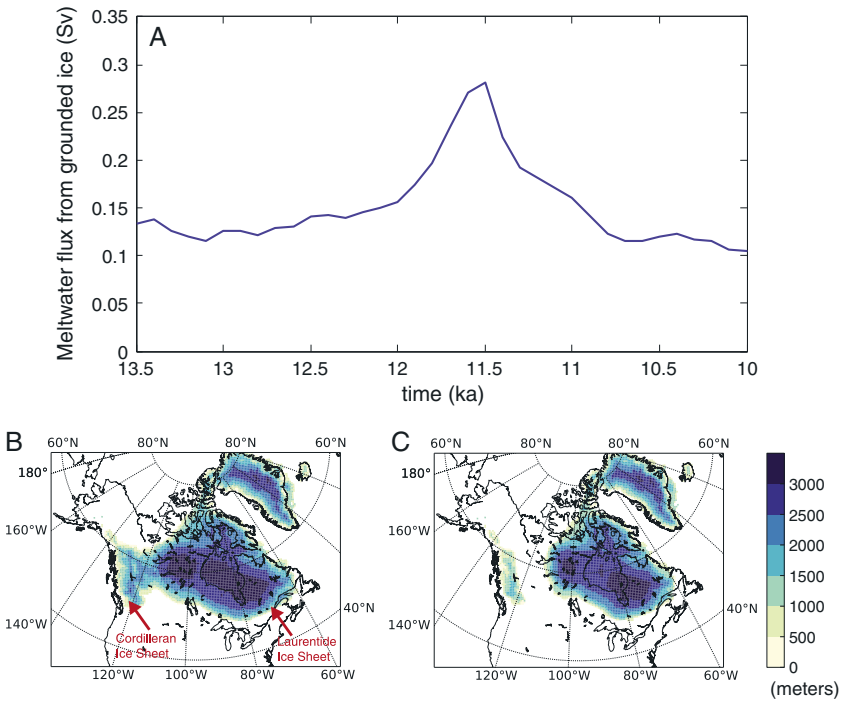

Figure 1. *Gregoire et al.*'s [2012] (G12) model of LIS, CIS, and GIS evolution through the meltwater pulse 1A event. (a) Meltwater flux from grounded ice (in sverdrups) as a function of model time (in kiloannum) before, during, and after the ice saddle collapse event they associate with MWP-1A. (b and c) Snapshots of grounded ice thickness over North America near the (Figure 1b) start and (Figure 1c) end of the saddle collapse.

due to Antarctic ice loss is insensitive to the viscous deformation of the solid Earth over the 500 year time window that we focus on. We scale the modeled pattern of sea level change from *Gomez et al.*'s [2013] ice model to consider contributions from the AIS with ESLE in the range of 0–13 m. An AIS retreat with an ESLE much greater than 1 m would likely involve a different melt geometry, which could produce biases in the sea level fingerprint. To assess this potential bias, we repeated our analysis replacing the Antarctic fingerprint with one produced by melting uniformly from the WAIS, and our conclusions were unaltered.

3. The Sea Level Fingerprint of the North American Ice Saddle Collapse

3.1. Evaluating Elastic and Viscous Effects

We begin with a prediction of sea level change across the 11.8–11.3 ka time window based on the G12 ice history and the VM2 viscosity model. Figure 2a shows this prediction after normalization by the ESLE associated with the total ice melt across this time window (10.47 m). Figure 2b shows the same prediction in the vicinity of the saddle collapse, resolving the near-field structure of the sea level change. The physics of this sea level change is well understood. In the near field of the saddle collapse, loss of gravitational attraction and solid Earth uplift dominate, driving a sea level fall with amplitude ~16 times the ESLE (~170 m). In contrast, sea level rises in the far field, reaching a peak value over 20% greater than the global average. The structure of the sea level change in the far field shows some interesting complexity. Ocean meltwater loading leads to a subsidence of the seafloor and a gradient in the computed sea level change close to shorelines. Moreover, the surface mass redistribution leads to true polar wander (a shift in the orientation of the rotation axis relative to the surface geography), and this drives much of the azimuthal asymmetry evident in the sea level prediction [*Milne and Mitrovica*, 1996].

Since we are considering the sea level change across a finite time interval in Figures 2a and 2b, the prediction may be decomposed into a component associated with instantaneous, elastic effects (henceforth the "elastic fingerprint") plus a component due to viscous effects associated with the full time history of the deglaciation up to 11.3 ka. These contributions (also normalized by the ESLE) are shown in Figures 2c and 2d, respectively.

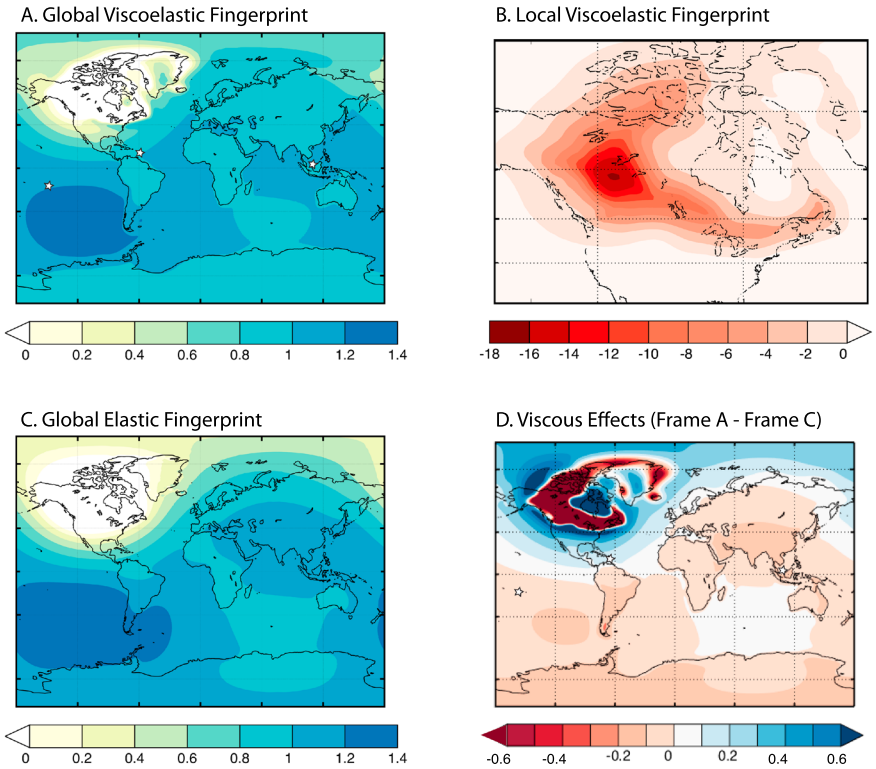

Figure 2. (a) Normalized sea level fingerprint computed for the saddle collapse between 11.8 and 11.3 ka in the G12 deglaciation model. (b) As in Figure 2a except that the plot focuses on the near field of the ice collapse. (c) Normalized sea level fingerprint computed assuming only elastic deformation of the Earth. (d) The difference between Figures 2a and 2c, isolating the contribution to the computed sea level change due to viscous deformation. The white stars in Figures 2a and 2d indicate the location of from left to right: Tahiti, Barbados, and Sunda Shelf.

In the vicinity of the regions of ice loss, the elastic fingerprint is characterized by widespread sea level fall that extends well beyond the margins of the ice loss: Note the extended and smooth zone of sea level fall in Figure 2c relative to Figure 2a. This sea level fall is due to a combination of crustal uplift and a fall in sea surface height due to gravitational effects associated with the ice loss. Within the near field, the difference between these two global fingerprints, which corresponds to the viscous signal (Figure 2d), is characterized by structure of smaller spatial scale, including postglacial uplift in response to ice melt from LGM to 11.3 ka in the G12 model, and subsidence at the periphery of these regions (blue zones in Figure 2d). The signal associated with the dynamics of the peripheral bulge extends to central America, where it contributes a normalized sea level rise of ~0.1–0.2.

Within the far field of the ice melting, the geographic variability in Figures 2c and 2d is of similar geometry, but the perturbations relative to the ESLE are of opposite sign. In Figure 2c, the sea level rise above the ESLE (i.e., above 1.0) within the far field is associated with gravitationally induced migration of water away from the near field. In contrast, the viscous signal involves a migration of water out of the far field and into near-field regions experiencing peripheral bulge subsidence. This effect, commonly called "ocean syphoning" [*Mitrovica and Milne*, 2002], leads to the large-scale drop in sea surface height (and consequently sea level fall) in Figure 2d.

Both Figures 2c and 2d also show the imprint of the true polar wander discussed in the context of Figure 2a. The saddle collapse drives an instantaneous perturbation of the rotation axis such that the north pole moves toward the zone of collapse and the south pole moves toward the Indian Ocean; this polar motion perturbs the centrifugal potential and contributes a sea level rise in the southeast Pacific and Asia and sea level fall in the Indian Ocean relative to the background trend (Figure 2c). In contrast, viscous adjustment associated with the full history of melting moves the pole in roughly the opposite direction, augmenting the background sea level fall due to syphoning in the south Pacific and Asia and countering it in the Indian Ocean, where a small sea level rise is predicted (Figure 2d).

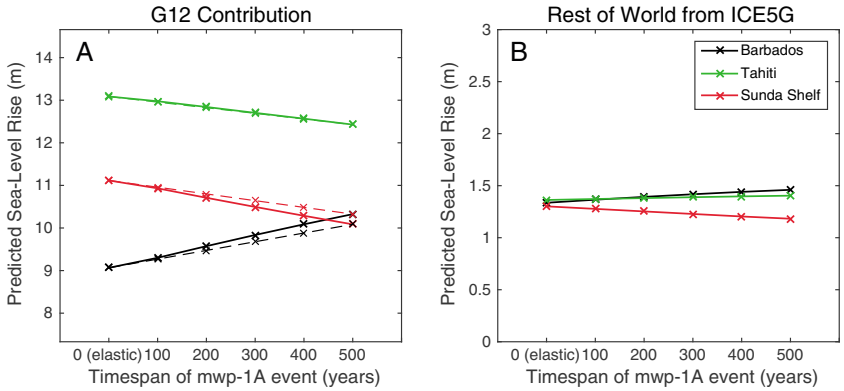

Figure 3. (a) Sea level rise predicted at Barbados (black lines), Tahiti (green lines), and Sunda Shelf (red lines) for the MWP-1A event in the G12 model of the LIS, CIS, and GIS (see Figures 1 and 2). (b) Sea level rise predicted at the same sites due to changes in ice cover outside of Greenland and North America during the MWP-1A event in the ICE-5G ice history (14.5–14.0 ka). Predictions are plotted as a function of the assumed duration of the event (in years), and calculations were performed using the VM2 (solid lines) and LM (dashed lines) mantle viscosity profiles.

In summary, the total sea level change across the MWP-1A event in the G12 model (Figure 2a) is dominated by the combined effect of eustasy and elastic deformation (Figure 2c). Viscous effects across the 11.8–11.3 ka time window of the simulation are, however, significant. These effects act to increase the predicted sea level rise in areas such as the Caribbean relative to Figure 2c, and they act to diminish the predicted sea level rise within the far field in nearly all other areas with the exception of the southern Indian Ocean.

3.2. Sensitivity to the Duration of MWP-1A

While viscous effects can have a significant impact on predictions of the sea level change associated with the MWP-1A event, the magnitude of this contribution will depend on the duration of the event, which is uncertain. Sampling issues in sea level records make it difficult to constrain the duration of the event; *Deschamps et al.* [2012] concluded, on the basis of the Tahiti record, that MWP-1A took place in less than ~340 years, but the duration could have been as short as a century or less. On the modeling side, the G12 ice history is characterized by a meltwater pulse of 10.47 m ESLE in 500 years, but this time scale could have been altered if missing or uncertain climatic and dynamical processes had been taken into account. For example, the Bølling warming is thought to have occurred at the time of the saddle collapse. If the event was included in the climate forcing applied to the ice sheet model, it could have accelerated the melting of the North American ice sheets.

To address this uncertainty, we have repeated the sea level calculations presented in Figure 2 for a suite of simulations in which the total change in ice volume between 11.8 and 11.3 ka (ESLE = 10.47 m) was applied over progressively shorter time windows ranging from 500 years (as in Figure 2a) to 0 year (as in Figure 2c). The ice history from 21 ka to 11.8 ka was unchanged in all the simulations. Predictions of the sea level change at Barbados, Tahiti, and Sunda Shelf for this sequence of simulations were calculated using both the VM2 and LM viscosity profiles (Figure 3a). A comparison of these results indicates that the magnitude of the signal due to viscous adjustments is relatively insensitive to the adopted viscosity model.

The predictions at all three sites vary linearly as the duration is increased from 0 (the purely elastic case) to 500 years. That is, the perturbation in the sea level prediction associated with viscous effects increases linearly over the range of durations considered in Figure 3. Barbados sits on the peripheral bulge of the saddle collapse, and thus, as discussed above, viscous effects contribute a sea level rise at this site. In contrast, viscous adjustments contribute a sea level fall at Tahiti and Sunda Shelf, which are in the far field of the saddle collapse. Thus, viscous effects bring predictions at Tahiti and Sunda Shelf closer to the Barbados predictions as the assumed duration of the event increases.

3.3. Other Sources of MWP-1A

In order to compare the predictions in Figure 3a to sea level observations, we must account for the contribution to MWP-1A from melting of ice outside of the G12 model domain. To this end, Figure 3b

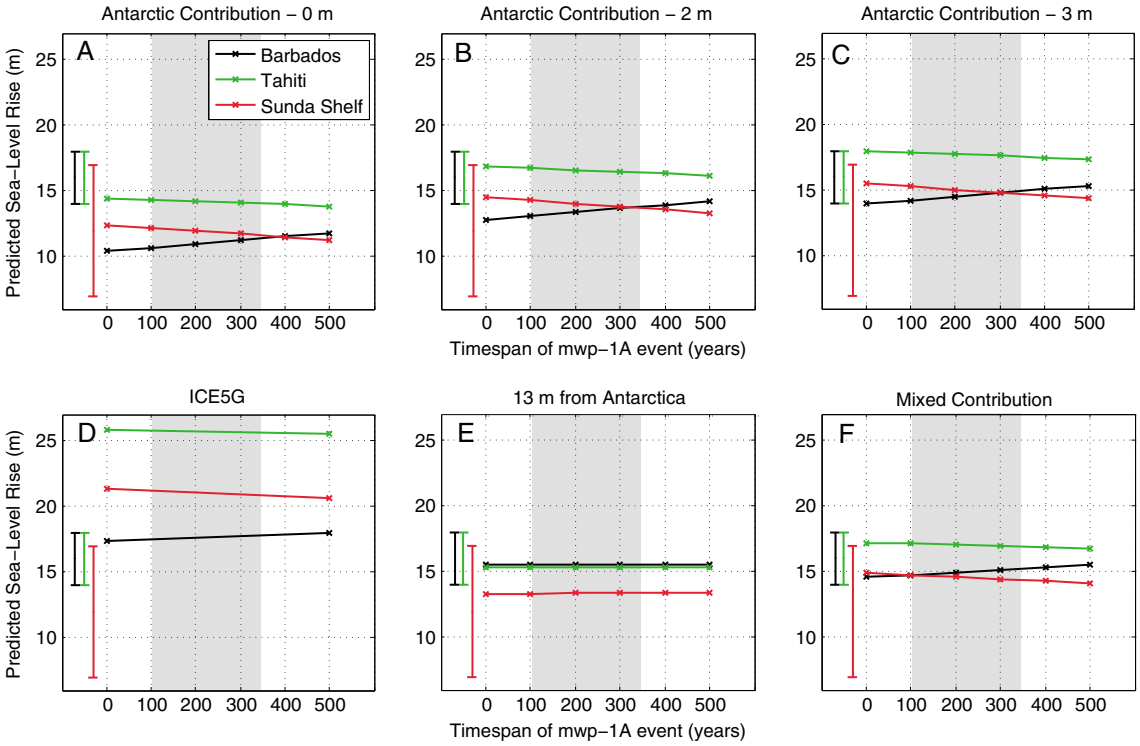

Figure 4. Total predicted sea level change across the MWP-1A time window at Barbados (black lines), Tahiti (green lines), and Sunda Shelf (red lines) as a function of the assumed duration of the event (in years). (a) Computed by adding the predicted sea level change from the G12 deglaciation model (Figure 3a) to the signal associated with melting (largely) from Eurasia across the 14.5–14.0 ka time window of the ICE-5G ice history (ESLE = 1.3 m; Figure 3b). (b) As in Figure 4a except that a contribution due to melting from the AIS with an ESLE of 2 m is added to the signal. (c) As in Figure 4b except that the AIS contribution is increased to an ESLE of 3 m. (d) Shows predictions that adopt the ice geometry from 14.5 to 14 ka in the ICE-5G history but vary the duration of the melt from 0 to 500 years. (e) As in Figure 4d but for a scenario with an ESLE of 13 m sourced entirely from the AIS. (f) As in Figure 4d except for a scenario that includes the ice sheet collapse in the G12 model (Figure 3a) scaled down to an ESLE of 7 m; melting from the AIS with an ESLE of 6 m; and a signal from Eurasian ice sheets and Patagonia (ESLE = 1.3; Figure 3b). All calculations adopt the VM2 mantle viscosity model. The vertical error bars on the left-hand side of each frame represent the observational constraint at the three sites, while the shaded region indicates the observational constraint on the duration of MWP-1A [*Deschamps et al.*, 2012].

shows predicted sea level changes from ice flux outside of North America and Greenland in the ICE-5G ice history across the 14.5–14.0 kyr time window. The melting is sourced mainly from Fennoscandia and the Barents Sea with a small contribution from Patagonia and has an ESLE of ~1.3 m. The signal is small and relatively insensitive to viscous effects.

4. MWP-1A Scenarios

Having evaluated sea level contributions from individual ice sheets, we can now consider various combinations of these signals. In Figure 4a, we sum the contributions to sea level change across MWP-1A at Barbados, Tahiti, and Sunda Shelf from the G12 deglaciation model (Figure 3a) and ice melting from Fennoscandia and the Barents Sea in the ICE-5G ice history (Figure 3b). The predicted sea level jumps at Sunda Shelf and Tahiti are consistent with the observed constraints, although the latter is at the lower bound of the preferred range cited by *Deschamps et al.* [2012]. In contrast, the computed jump at Barbados is less than the associated observation, regardless of the assumed duration of MWP-1A.

Figure 4a includes no contribution from the AIS. To consider this possible contribution, a gravitationally self-consistent signal from progressively higher rates of melting from the AIS was added to the results in Figure 4a. For Antarctic melting with an ESLE of 2 m (Figure 4b), the predicted sea level jumps at Tahiti and Sunda Shelf remain within the associated observational constraints, and the total signal at Barbados begins to skirt the lower bound of the constraint for this site (14 m) for a MWP-1A duration of ~500 years. Increasing the AIS melting to an ESLE of 3 m also satisfies the observational constraints (Figure 4c) however the prediction at Tahiti is, in this case, at the upper bound of the observations.

The fingerprint of melting from the Eurasian ice sheets is similar to the fingerprint of melting from the AIS at the three far field sites we are considering (Barbados, Sunda Shelf, and Tahiti), and so these melt contributions cannot be rigorously separated given current observational uncertainties in regard to the sea level change across MWP-1A. We conclude that a combination of the saddle collapse scenario of G12 (ESLE = 10.5 m) and additional melting from other ice sheets equivalent to an ESLE of ~3–4 m satisfies the observational constraints. We note that the scenarios presented in Figures 4b and 4c are consistent with ice sheet modeling by *Golledge et al*. [2014] who conclude that the AIS contributed up to 2 m ESLE in the 340 years spanning MWP-1A and ~2–4 m over a broader, 2 kyr time window across the event.

As a point of comparison, Figure 4d shows the sea level rise at the three far-field sites predicted using the ICE-5G ice history and the VM2 viscosity profile. MWP-1A takes place between 14.5 ka and 14.0 ka in the ICE-5G reconstruction and involves a eustatic sea level rise of ~22 m, 90% of which is sourced to the LIS. The set of predictions in Figure 4d are generated by reducing the duration of the melt event from 500 years (as in the model) to 0 year. These predictions significantly misfit the observed sea level jumps at Sunda Shelf and Tahiti, and they are at the upper bound of the Barbados constraint. Note that the prediction for Tahiti is nearly 50% higher than that at Barbados [*Clark et al*., 2002]. This large misfit as compared to the saddle collapse scenario is due to a combination of the difference in the geometry and magnitude of ice loss between the two scenarios. We conclude that this LIS-dominated collapse scenario is ruled out by the data [*Clark et al*., 2002; *Deschamps et al*., 2012] and that the fit to the observations is significantly improved by moving the dominant source of the meltwater pulse from Laurentia to the saddle joining the LIS and CIS.

Figure 4e shows the predicted sea level rise for a melt scenario with an ESLE of 13 m sourced entirely to the AIS. This scenario fits the observations at Barbados, Sunda Shelf, and Tahiti. This fit has motivated suggestions that the AIS may have been the dominant source of MWP-1A [*Clark et al*., 2002; *Deschamps et al*., 2012]. A comparison of this result with Figure 4b indicates that further refinements in the existing constraints on the sea level jump across MWP-1A at Barbados, Sunda Shelf, and Tahiti and tighter bounds on the duration of the event, or new constraints obtained from other sites [e.g., the Argentine Shelf; *Clark et al*., 2002], are necessary to unambiguously fingerprint (using sea level) the source(s) of MWP-1A.

To emphasize this nonuniqueness, we tested a final scenario (Figure 4f), where we scaled the saddle collapse scenario down to an ESLE of 7 m (from 10.5 m in Figure 1) and added additional melting from both Antarctica (ESLE of 6 m) and Eurasia (as in Figure 3b; ESLE of 1.3 m). The sea level rise predicted at Barbados, Tahiti, and Sunda Shelf for this scenario also satisfies the available observational constraints.

5. Discussion

Could the North American and Greenland meltwater pulses have been much larger or smaller than the event simulated in G12? Many climatic and glaciological processes influence the volume of the meltwater pulse, but the largest source of uncertainty in this modeling is related to the ~3 kyr delay in the timing of the modeled event relative to the actual timing of MWP-1A, which could have acted either to increase or decrease the amplitude of the pulse. The delay in the model simulation could affect whether other sectors of the ice sheet retreated, leading up to and during the saddle collapse. In addition, the climate was warmer at this later time and this might have resulted in an overestimation of the melt volume.

An additional factor, which may be important in determining the volume of the pulse, is the adopted definition for its duration, which is subjective. In observational records, the start and end dates of the meltwater pulse are identified on the basis of a detectable increase in the slope of the sea level change. In other words, the melt rate has to increase significantly compared to the background melting of ice sheets in order for the event to be detected in sea level records. If we assume that melt rates should be at least 1.5 times larger than the background melt rates, then the meltwater pulse from the G12 model lasts 500 years (11.8–11.3 ka) and raises global mean sea level by 10.5 m. If this factor is increased to 1.6 times the background rate, then the signal observed in the sea level record would only last 300 years (11.7–11.4 ka) and correspond to 6.8 m ESLE.

6. Conclusions

We have predicted sea level changes associated with the G12 model of the evolution of the LIS, CIS, and GIS since LGM. Our results show that a saddle collapse between the LIS and CIS (ESLE~10.5 m) could have been

the dominant source of MWP-1A on the basis of fits between our predictions and the observed sea level changes at Barbados, Sunda Shelf, and Tahiti. However, our analysis also confirms that these observations are well fit by a scenario in which changes in the AIS ice cover dominate the meltwater budget. Discriminating between these, and perhaps other scenarios, will require improvements to the existing database of high-resolution observational constraints.

The enigma concerning the source(s) of MWP-1A is deepened by independent analyses based on other types of data and modeling. For example, a dominant AIS source for the event is inconsistent with recent modeling of the geophysical signatures of AIS deglaciation since LGM [*King et al*., 2012; *Ivins et al*., 2013], as well as coupled ice sheet-sea level modeling of the AIS [*Gomez et al*., 2013]. A dominant meltwater source from the saddle collapse would avoid these inconsistencies. Oxygen isotopic signatures of drainage through the Mississippi River Basin since LGM recorded in deep-sea cores from the Gulf of Mexico suggest a minimal part of MWP-1A (between 0.66 and 2.7 m of ESLE) was routed toward the Mississippi [*Carlson*, 2009; *Wickert et al*., 2013]. An ice saddle collapse with an ESLE rise as predicted in the G12 model (~10.5 m), but timed to coincide with MWP-1A, may therefore be inconsistent with these data if a large part of the melting was routed toward the Mississippi. *Wickert* [2014] finds that about two thirds of the North American ice sheet melt in the G12 model is routed toward the Arctic Ocean, where drainage history is poorly constrained. However, such a release of freshwater into the Arctic may have wider implications for ocean circulation, and in particular for the Atlantic Meridional Overturning Circulation [e.g., *Hu et al*., 2010]. Further work is clearly necessary to robustly resolve this outstanding issue in ice age climate. Our approach of testing individual scenarios (Figure 4) could be expanded into a more rigorous Bayesian analysis of all the possible distributions for MWP-1A sources once observational constraints on the duration and magnitude of the event are sufficiently refined.

Acknowledgments

We thank the reviewers, Peter Clark and Pippa Whitehouse, for their helpful suggestions. Relative sea level data used in this paper are shown in Figure 4 and available upon request from Glenn Milne and in the following reference: Deschamps, P., Durand, N., Bard, E., Hamelin, B., Camoin, G., Thomas, A. L., Henderson, G. M., Okuno, J., Yokoyama, and Y., 2012. Ice sheet collapse and sea level rise at the Bolling warming 14,600 years ago. Nature 483, 559–564.

The Editor thanks Peter Clark and one anonymous reviewer for their assistance in evaluating this paper.

References

Andrews, J. T., H. Erlenkeuser, K. Tedesco, A. E. Aksu, and A. J. T. Jull (1994), Late Quaternary (Stages 2 and 3) meltwater and Heinrich events, northwest Labrador Sea, *Quat. Res.*, *41*, 26–34.

Bard, E., B. Hamelin, R. G. Fairbanks, and A. Zinlder (1990), Calibration of the 14C time scale over the past 30,000 years using mass spectrometric U-Th ages from Barbados corals, *Nature*, *345*, 405–410.

Bard, E., B. Hamelin, and D. Delanghe-Sabatier (2010), Deglacial meltwater pulse 1B and younger dryas sea levels revisited with boreholes at Tahiti, *Science*, *327*, 1235–1237.

Bassett, S. E. (2005), Ice sheet and solid Earth influences on far-field sea level histories, *Science*, *309*, 925–928.

Briggs, R. D., D. Pollard, and L. Tarasov (2014), A data-constrained large ensemble analysis of Antarctic evolution since the Eemian, *Quat. Sci. Rev.*, *103*, 91–115.

Carlson, A. E. (2009), Geochemical constraints on the Laurentide Ice Sheet contribution to meltwater pulse 1A, *Quat. Sci. Rev.*, *28*, 1625–1630.

Clark, P. U., J. X. Mitrovica, G. A. Milne, and M. E. Tamisiea (2002), Sea level fingerprinting as a direct test for the source of global meltwater pulse IA, *Science*, *295*, 2438–2441.

Deschamps, P., N. Durand, E. Bard, B. Hamelin, G. Camoin, A. L. Thomas, G. M. Henderson, J. Okuno, and Y. Yokoyama (2012), Ice sheet collapse and sea level rise at the Bolling warming 14,600 years ago, *Nature*, *483*, 559–564.

Dyke, A. S. (2004), An outline of North American deglaciation with emphasis on central and northern Canada, in *Quaternary Glaciations-Extant and Chronology. Part II: North America*, Dev. Quat. Sci., vol. 2, edited by J. Ehlers and P. L. Gibbard, pp. 373–424, Elsevier Science and Technology Books, Amsterdam.

Dziewonski, A. M., and D. L. Anderson (1981), Preliminary reference Earth model, *Phys. Earth Planet. Inter.*, *25*, 297–356.

Fairbanks, R. G. (1989), A 17,000-year glacio-eustatic sea level record: Influence of glacial melting rates on the younger dryas event and deep-ocean circulation, *Nature*, *342*, 637–642.

Fairbanks, R. G., C. D. Charles, and J. D. Wright (1992), Origin of global meltwater pulses, in *Four Decades of Radiocarbon Studies*, pp. 473–500, Springer, New York.

Golledge, N. R., L. Menviel, L. Carter, C. J. Fogwill, M. H. England, G. Cortese, and R. H. Levy (2014), Antarctic contribution to meltwater pulse 1A from reduced Southern Ocean overturning, *Nat. Commun.*, *5*, 5107, doi:10.1038/ncomms6107.

Gomez, N., J. X. Mitrovica, M. E. Tamisiea, and P. U. Clark (2010), A new projection of sea level change in response to collapse of marine sectors of the Antarctic Ice Sheet, *Geophys. J. Int.*, *180*, 623–634.

Gomez, N., D. Pollard, and J. X. Mitrovica (2013), A 3-D coupled ice sheet-sea level model applied to Antarctica over the last 40 kyr, *Earth Planet. Sci. Lett.*, *384*, 88–99.

Gregoire, L. J., A. J. Payne, and P. J. Valdes (2012), Deglacial rapid sea level rises caused by ice sheet saddle collapses, *Nature*, *487*, 219–222.

Hanebuth, T., K. Stattegger, and P. M. Grootes (2000), Rapid flooding of the Sunda Shelf: A late-glacial sea level record, *Science*, *288*, 1033–1035.

Hu, A., G. A. Meehl, B. L. Otto-Bliesner, C. Waelbroeck, W. Han, M. F. Loutre, K. Lambeck, J. X. Mitrovica, and N. Rosenbloom (2010), Influence of Bering Strait flow and North Atlantic circulation on glacial sea level changes, *Nat. Geosci.*, *3*, 118–121.

Ivins, E. R., T. S. James, J. Wahr, O. Schrama, J. Ernst, F. W. Landerer, and K. M. Simon (2013), Antarctic contribution to sea level rise observed by GRACE with improved GIA correction, *J. Geophys. Res. Lett.*, *118*, 1–16, doi:10.1002/jgrb.50208.

Keigwin, L. D., and G. A. Jones (2010), Deglacial climatic oscillations in the Gulf of California, *Paleoceanography*, *5*, 1009–1023, doi:10.1029/PA005i006p01009.

Kendall, R. A., J. X. Mitrovica, and G. A. Milne (2005), On post-glacial sea level - II. Numerical formulation and comparative results on spherically symmetric models, *Geophys. J. Int.*, *161*, 679–706.

Kennett, J. P., and N. J. Shackleton (1975), Laurentide Ice Sheet meltwater recorded in Gulf of Mexico deep-sea cores, *Science*, *188*, 147–150.

King, M. A., R. J. Bingham, P. Moore, P. L. Whitehouse, M. J. Bentley, and G. A. Milne (2012), Lower satellite-gravimetry estimates of Antarctic sea level contribution, *Nature*, *491*, 586–589.

Lambeck, K., H. Rouby, A. Purcell, Y. Sun, and M. Sambridge (2014), Sea level and global ice volumes from the Last Glacial Maximum to the Holocene, *Proc. Natl. Acad. Sci. U.S.A.*, *111*, 15,296–15,303.

Leventer, A., D. F. Williams, and J. P. Kennett (1982), Dynamics of the Laurentide ice sheet during the last deglaciation: Evidence from the Gulf of Mexico, *Earth Planet. Sci. Lett.*, *59*, 11–17.

Liu, J., G. A. Milne, R. E. Kopp, and I. Shennan (2013), Constraining the source distribution of MWP-1A using near- and far-field data and modelling constraints, EOS Transactions AGU, Fall Meeting Supplement, Abstract PP51D-07.

Milne, G. A., and J. X. Mitrovica (1996), Post-glacial sea level variations on a rotating Earth: First results from a gravitationally self-consistent sea level equation, *Geophys. J. Int.*, *126*, F13–F20.

Mitrovica, J. X., and A. M. Forte (2004), A new inference of mantle viscosity based upon joint inversion of convection and glacial isostatic adjustment data, *Earth Planet. Sci. Lett.*, *225*, 177–189.

Mitrovica, J. X., and G. A. Milne (2002), On the origin of late Holocene sea level highstands within equatorial ocean basins, *Quat. Sci. Rev.*, *21*, 2179–2190.

Munyikwa, K., J. K. Feathers, T. M. Rittenour, and H. K. Shrimpton (2011), Constraining the Late Wisconsinan retreat of the Laurentide Ice Sheet from western Canada using luminescence ages from postglacial aeolian dunes, *Quat. Geochronol.*, *6*, 407–422.

Peltier, W. R. (2004), Global glacial isostasy and the surface of the ice-age Earth: The ICE-5G (VM2) model and GRACE, *Annu. Rev. Earth Planet. Sci.*, *32*, 111–149.

Weaver, A. J., O. A. Saenko, P. U. Clark, and J. X. Mitorivca (2003), Meltwater pulse 1A from Antarctica as a trigger of the Bolling-Allerod warm interval, *Science*, *299*, 1709–1713.

Whitehouse, P. L., M. J. Bentley, and A. M. Le Brocq (2012), A deglacial model for Antarctica: Geological constraints and glaciological modelling as a basis for a new model of Antarctic glacial isostatic adjustment, *Quat. Sci. Rev.*, *32*, 1–24.

Wickert, A. D. (2014), Impacts of Pleistocene glaciation and its geophysical effects on North American river systems, PhD dissertation, p. 153, Univ. of Colorado, Boulder.

Wickert, A. D., J. X. Mitrovica, C. Williams, and R. S. Anderson (2013), Gradual demise of a thin southern Laurentide Ice Sheet recorded by Mississippi drainage, *Nature*, *502*, 668–671.